

Reliable Grid Forecasting: State Space Models for Safety-Critical Energy Systems

Sunki Hong and Jisoo Lee

Gramm AI.

*Corresponding author(s). E-mail(s): jisoo@gramm.ai;

Contributing authors: sunki@gramm.ai;

Abstract

Accurate grid load forecasting is safety-critical: under-predictions risk supply shortfalls, while symmetric error metrics can mask this operational asymmetry. We introduce an operator-legible evaluation framework—Under-Prediction Rate (UPR), tail Reserve_{99.5}[%] requirements, and explicit inflation diagnostics (Bias_{24h}/OPR)—to quantify one-sided reliability risk beyond MAPE.

Using this framework, we evaluate state space models (Mamba variants) and strong baselines on a weather-aligned California Independent System Operator (CAISO) dataset spanning Nov 2023–Nov 2025 (84,498 hourly records across 5 regional transmission areas) under a rolling-origin walk-forward backtest. We develop and evaluate thermal-lag-aligned weather fusion strategies for these architectures.

Our results demonstrate that standard accuracy metrics are insufficient proxies for operational safety: models with comparable MAPE can imply materially different tail reserve requirements (Reserve_{99.5}[%]). We show that explicit weather integration narrows error distributions, reducing the impact of temperature-driven demand spikes. Furthermore, while probabilistic calibration reduces large-error events, it can induce systematic schedule inflation. We introduce Bias/OPR-constrained objectives to enable auditable trade-offs between minimizing tail risk and preventing trivial over-forecasting.

Keywords: Load forecasting, state space models, Mamba, deep learning, probabilistic forecasting, California grid, CAISO

1 Introduction

Short-term load forecasting (STLF) underpins electricity grid operations, governing unit commitment, economic dispatch, and reserve scheduling [1]. The consequences are significant: under-prediction risks cascading blackouts, while over-prediction incurs unnecessary costs and emissions.

California’s grid exemplifies the challenges facing high-renewable systems. Utility-scale solar and wind contribute roughly one quarter of CAISO system energy [2], with behind-the-meter (BTM) solar capacity exceeding 17 GW in California [3]. This invisible generation creates the “duck curve”—deep midday net load trough followed by steep evening ramps—that evolves annually as BTM capacity expands. Compounding this non-stationarity, climate-driven extreme weather events increasingly trigger non-linear demand spikes that defy historical patterns [4].

Existing forecasting methods face fundamental limitations. Statistical approaches (ARIMA) cannot capture non-linear weather dependencies [5]. Recurrent networks (LSTMs) struggle with long-range dependencies due to vanishing gradients. Transformer architectures address this but introduce quadratic $O(n^2)$ complexity, limiting practical context lengths for capturing multi-week seasonal patterns [6].

State space models (SSMs) offer a compelling path to reliability. By achieving linear $O(n)$ scaling, Mamba [7] allows for extended historical contexts and lower inference latency, freeing computational budget for robust uncertainty quantification and ensemble methods. However, Mamba’s ability to maintain safety margins in regional grid forecasting—characterized by asymmetric error costs and heteroscedasticity—remains unexplored.

We present a systematic evaluation of Mamba architectures for reliable California grid load forecasting. Benchmarking against iTransformer and the foundation model Chronos, we shift the evaluation focus from pure accuracy to *operational safety*. Our walk-forward results highlight that accuracy alone is not a sufficient proxy for operational risk: Reserve $_{99.5}^{\%}$ can vary substantially across models even when MAPE is comparable. Furthermore, we demonstrate that explicit weather integration is critical for safety by narrowing error distributions and reducing extreme error events (Section 6.3).

Contributions

To move beyond symmetric accuracy metrics toward operator-relevant reliability for California grid forecasting, we make the following contributions:

1. **Grid-Specific Evaluation Framework.** We formalize operational risk metrics (Under-Prediction Rate, tail Reserve $_{99.5}^{\%}$ requirements, Bias/OPR diagnostics) that capture asymmetric operational costs and prevent “fake safety” via systematic forecast inflation (Section 2.3).
2. **Weather Integration for SSMs.** We develop (Section 4.2) and systematically evaluate (Section 6.3) thermal-lag-aligned weather fusion strategies for Mamba architectures, improving robustness by narrowing error distributions and reducing extreme errors.

3. **Loss vs. Safety Analysis.** We show that proper probabilistic calibration (multi-quantile pinball) can reduce large-error events on fixed evaluation splits, but can also introduce systematic inflation unless Bias/OPR are explicitly constrained and jointly reported with tail-risk metrics (Section 6).

2 Background

2.1 State Space Models

State space models (SSMs) provide a principled framework for modeling sequential data through continuous-time dynamical systems. The general linear SSM is defined by the following ordinary differential equations:

$$h'(t) = Ah(t) + Bx(t), \quad y(t) = Ch(t) + Dx(t) \quad (1)$$

where $x(t) \in \mathbb{R}$ is the input signal, $h(t) \in \mathbb{R}^N$ is the latent state with dimension N , and $y(t) \in \mathbb{R}$ is the output. The matrices $A \in \mathbb{R}^{N \times N}$, $B \in \mathbb{R}^{N \times 1}$, $C \in \mathbb{R}^{1 \times N}$, and $D \in \mathbb{R}$ are learnable parameters.

For discrete-time computation on sampled data, the continuous SSM must be discretized. Using zero-order hold discretization with time step Δ , the discrete-time SSM becomes:

$$h_k = \bar{A}h_{k-1} + \bar{B}x_k, \quad y_k = Ch_k \quad (2)$$

where $\bar{A} = \exp(\Delta A)$ and $\bar{B} = (\Delta A)^{-1}(\exp(\Delta A) - I) \cdot \Delta B$.

Selective state spaces. Traditional SSMs employ time-invariant (LTI) parameters. The Mamba architecture [7] introduces a selective mechanism that makes these parameters input-dependent:

$$B_k = s_B(x_k), \quad C_k = s_C(x_k), \quad \Delta_k = \text{softplus}(s_\Delta(x_k)) \quad (3)$$

where s_B , s_C , and s_Δ are learned projections. This selectivity enables the model to filter relevant information while forgetting irrelevant context, addressing a fundamental limitation of prior SSMs.

Suitability for grid data. Recent analysis by Wang et al. [8] identifies conditions where Mamba outperforms Transformers: datasets with “numerous variates, most of which are periodic.” Grid load data matches this characterization precisely—highly periodic signals (daily/weekly cycles) across multiple spatial nodes. Mamba’s selective state mechanism encodes these rhythmic dependencies while filtering stochastic noise.

Computational complexity. SSMs achieve $O(n)$ complexity versus $O(n^2)$ for self-attention. Menati et al. [9] demonstrate that context windows of 240+ hours are optimal for capturing multi-scale grid dynamics—a length computationally prohibitive for standard Transformers.

2.2 Load Forecasting Fundamentals

Definition and Horizons. Short-term load forecasting (STLF) encompasses prediction of electricity demand from hours to days ahead [10]. Different forecast horizons

serve distinct operational purposes: 1-hour for real-time dispatch, 4–6 hours for unit commitment, and 12–24 hours for day-ahead market operations.

Multi-Periodicity. Electricity load exhibits strong multi-periodic patterns (daily, weekly, annual). Our choice of 240-hour (10-day) context length ensures capture of at least one complete weekly cycle.

Evaluation Metrics. For load forecasting with positive data, mean absolute percentage error (MAPE) is the standard metric:

$$\text{MAPE} = \frac{100}{n} \sum_{i=1}^n \left| \frac{y_i - \hat{y}_i}{y_i} \right| \quad (4)$$

2.3 Grid-Specific Evaluation Metrics

Standard metrics like MAPE and RMSE treat forecast errors symmetrically: an over-prediction of 100 MW is penalized identically to an under-prediction of 100 MW. For grid utility operators, however, the economic and reliability consequences of these errors are fundamentally asymmetric [1].

2.3.1 Operational Cost Asymmetry

- **Over-Prediction (False Positive):** If the model predicts higher load than the actual demand, the utility commits excess generation. This results in financial loss (wasted fuel, curtailment costs) but rarely threatens system stability.
- **Under-Prediction (False Negative):** If the model predicts lower load than the actual demand, the utility may face a supply shortfall. This necessitates deploying expensive fast-ramping reserves (e.g., peaker plants), purchasing emergency power at spot market caps (often \$1,000+/MWh), or in extreme cases, initiating rolling blackouts.

Standard MAPE is therefore insufficient for operational validation. To address this, we introduce a suite of grid-specific metrics:

2.3.2 Proposed Metrics

Under-Prediction Rate (UPR). The frequency of under-estimation events represents the probability of needing real-time upward dispatch:

$$\text{UPR} = \frac{1}{n} \sum_{i=1}^n \mathbb{I}(y_i > \hat{y}_i) \times 100\% \quad (5)$$

A naive model might achieve low MAPE by constantly under-predicting (taking the median); UPR exposes this risky behavior.

Over-Prediction Rate (OPR). The frequency of over-forecasting events exposes systematic inflation in the scheduled (median) forecast:

$$\text{OPR} = \frac{1}{n} \sum_{i=1}^n \mathbb{I}(\hat{y}_i > y_i) \times 100\% \quad (6)$$

In safety-critical settings, OPR provides a simple operator-legible diagnostic for whether improvements in one-sided tail risk are achieved by trivial over-scheduling.

Upward Reserve Requirement (Reserve_{99.5}[%]). The additional upward capacity required to cover 99.5% of the *under-forecast* error distribution. We use the 99.5th percentile as a practical tail-risk proxy motivated by probabilistic adequacy practice (e.g., LOLE-style planning criteria; [11]). We report this both in megawatts (MW) and as a percentage of the point forecast (scale-free):

$$\text{Reserve}_{99.5}^{\text{MW}} = \text{Percentile}_{99.5}(\max(0, y - \hat{y})) \quad (7)$$

$$\text{Reserve}_{99.5}^{\%} = 100 \times \text{Percentile}_{99.5}\left(\max\left(0, \frac{y - \hat{y}}{\hat{y}}\right)\right) \quad (8)$$

Adding Reserve_{99.5}^{MW} to the point forecast covers 99.5% of historical under-prediction events at the evaluated horizon. We report both MW and percentage: MW is normalization-free, while the percentage form is directly interpretable as an *add-on* to the scheduled point forecast. Because percentage-normalized reserve can be biased by systematic forecast inflation, we interpret Reserve_{99.5}[%] jointly with UPR and explicit bias diagnostics (Bias_{24h} / OPR) to ensure improvements do not come from trivial over-forecasting.

2.3.3 Motivating Example

To illustrate the operational reality of these metrics, we examine empirical results (detailed later in Table 2) where tail-risk metrics and bias diagnostics move in different directions. For example, a model trained with a tail-focused loss might ostensibly reduce reserve requirements (Reserve_{99.5}[%]), but do so by simply inflating the entire forecast—increasing Bias_{24h} and Over-Prediction Rate (OPR) to unacceptable levels. This motivates our core reporting principle: any improvement in one-sided risk metrics must be interpreted jointly with bias diagnostics to avoid “fake safety” via systematic inflation.

2.3.4 Differentiable Surrogates for Risk Metrics

While UPR and tail reserve requirements are excellent for evaluation, they are non-differentiable and difficult to optimize directly. To bridge this gap, we employ a **Bias-Constrained Probabilistic Objective** (detailed in Section 4.3) as a differentiable surrogate during training. This objective combines a weighted multi-quantile pinball loss to learn a calibrated distribution with explicit hinge penalties on bias and over-prediction rate to prevent systematic forecast inflation.

In principle, emphasizing upper-tail quantiles increases the gradient penalty on under-predictions relative to over-predictions, aligning learning with asymmetric operational costs. However, as we demonstrate in Section 6, single-quantile training can be “gamed”; our constrained formulation (Section 4.3) ensures that improvements in tail risk do not come at the expense of acceptable schedule bias.

2.4 Value-Oriented Learning

Traditional forecasting objectives (MSE/MAPE) operate under the assumption that prediction accuracy proxies decision quality. However, in grid operations, the cost function is highly asymmetric and constrained. The “Value-Oriented” or “Smart Predict-then-Optimize” paradigm [12] challenges the separation of prediction and downstream optimization, proposing that models should be trained to minimize the final operational cost. While theoretically optimal, full end-to-end bilevel optimization is often computationally intractable for large-scale deep learning. In this work, we adopt a scalable realization of this philosophy: instead of embedding the full extensive-form optimization solver, we encode the operational value function directly into a **bias-constrained probabilistic objective** (Section 4.3).

3 Related Work

3.1 Deep Learning for Time Series

Deep learning has systematically displaced statistical methods (ARIMA, SVR) for short-term load forecasting due to its superior ability to model non-linear relationships. Current research focuses on two primary paradigms for long-context multivariate modeling:

Transformer-based Approaches. Computing global attention allows Transformers to capture long-range dependencies, but with $O(n^2)$ complexity. Two main strategies have emerged to handle multivariate data:

- *Channel Independence:* Models like **PatchTST** [13] treat multivariate time series as independent channels and segment them into patches. This reduces complexity and represents the current state-of-the-art for Transformer accuracy, though it sacrifices explicit cross-variable correlation modeling.
- *Multivariate Attention:* Models like **iTransformer** [14] explicitly model correlations between variables by inverting tokenization (embedding time steps as features). We study iTransformer as a primary baseline because its explicit modeling of spatial correlations (e.g., between load and weather variables) offers a direct contrast to the implicit state mixing of Mamba.

Efficient Sequence Modeling (SSMs). State space models offer a fundamentally different approach. Instead of the quadratic global attention of Transformers, SSMs like Mamba [7] employ a recurrent mode with input-dependent selection, achieving linear $O(n)$ scaling. This efficiency allows for significantly longer context windows (240+ hours) on the same hardware, potentially capturing seasonal patterns that are computationally prohibitive for attention-based models.

Linear Models. Recent work has challenged the necessity of deep learning for time series forecasting. DLinear [15] demonstrates that simple linear models often match or exceed Transformer performance on standard benchmarks, raising questions about architectural complexity. However, linear models cannot capture non-linear temperature-load relationships that dominate during extreme weather events—precisely when forecast accuracy is most critical for grid operations. While recent “value-oriented”

and end-to-end approaches propose embedding optimization layers directly into the training loop [12], these methods can be computationally prohibitive for large-scale deep learning sequence models. We instead propose a bias-constrained objective as a scalable, differentiable surrogate to align training with asymmetric operational costs. Our evaluation focuses on models capable of learning these non-linear interactions while maintaining computational tractability.

This work systematically evaluates whether the theoretical efficiency advantage of Mamba translates to superior accuracy on complex, real-world grid data compared to the expressive power of multivariate Transformers.

3.2 State Space Models for Time Series

The Structured State Space (S4) model [16] introduced efficient long-range sequence modeling through careful parameterization of continuous-time state spaces. Mamba [7] extended this framework with input-dependent (selective) parameters, enabling content-aware filtering that improves performance on language and genomics tasks. For time series specifically, S-Mamba [8] demonstrated that Mamba architectures excel on datasets with “numerous variates, most of which are periodic”—a characterization that matches grid load data. PowerMamba [9] introduced bidirectional processing and series decomposition specifically for energy applications, showing that 240+ hour context windows are optimal for capturing multi-scale grid dynamics.

3.3 End-to-End and Value-Oriented Learning

Recent advancements in "Smart Predict-then-Optimize" (SPO) have challenged the traditional separation of forecasting and decision-making. Value-oriented approaches [12] propose bi-level optimization frameworks where the forecasting model is updated based on the quality of downstream decisions (e.g., unit commitment costs) rather than proxy metrics like MSE. Similarly, end-to-end structural learning [17] embeds differentiable optimization layers to disentangle unobservable components (like baseline demand vs. price response) from aggregate signals.

Our work builds on these philosophies but focuses on *scalability*. Instead of solving extensive optimization problems within the training loop—which is often prohibitive for large-scale transformers—we propose a **bias-constrained probabilistic objective** as a differentiable surrogate that aligns the model with asymmetric operational values while maintaining the efficiency of standard backpropagation.

3.4 Weather-Integrated Forecasting

The relationship between weather and electricity demand is well-established [1]. Temperature-based load models form the basis of many operational forecasting systems, with heating and cooling degree days serving as primary predictors. However, integrating weather into deep learning architectures remains challenging due to temporal misalignment: building thermal mass introduces response lags of 2–6 hours between temperature changes and load response [18]. Prior work has addressed this through feature engineering and attention-based fusion strategies [5], but systematic evaluation of weather integration strategies for state space models is lacking.

3.5 Foundation Models for Time Series

Pre-trained foundation models have recently emerged as alternatives to task-specific architectures. Chronos [19] adapts language model pre-training to time series through quantization, demonstrating strong zero-shot performance on diverse forecasting benchmarks. However, the effectiveness of foundation models on domain-specific tasks with strong exogenous dependencies (e.g., weather-driven load) remains an open question, as these models typically lack mechanisms for incorporating auxiliary covariates.

4 Methodology

4.1 Model Architectures

We evaluate three Mamba-based architectures representing different design philosophies within the state space model paradigm, alongside the iTransformer baseline.

4.1.1 S-Mamba: The Linear-Time Baseline

S-Mamba [8] represents a minimalist approach to state space modeling. It adapts the standard Mamba block for time series via a simple encoder-decoder structure: a linear projection embeds the input sequence into a hidden state D , followed by stacked Mamba layers.

The primary goal of S-Mamba is to test whether the core selective state space mechanism alone—without complex decomposition or attention—is sufficient to model grid dynamics. Its design prioritizes computational efficiency ($O(n)$ complexity) above all else, making it an ideal candidate for resource-constrained edge deployment (0.08ms inference latency).

4.1.2 PowerMamba: Physics-Aware Decomposition

PowerMamba [9] addresses a specific limitation of standard SSMs: the difficulty of modeling disparate frequencies (e.g., long-term trend vs. daily seasonality) within a single state vector.

PowerMamba introduces two critical innovations for energy data:

- *Series Decomposition*: It splits the input into "Trend" (low-frequency) and "Seasonal" (high-frequency) components, and processes them via independent Mamba encoders. This explicitly separates the "duck curve" drift from daily load cycles.
- *Bidirectionality*: Unlike language modeling where causality is strict (future cannot affect past), time series analysis benefits from looking forward (e.g., smoothing). PowerMamba processes sequences in both forward and backward directions to capture a holistic temporal context.

4.1.3 Mamba-ProbTSF: Probabilistic Output Heads

Grid operators rarely make decisions based on a single deterministic number; they require confidence intervals to schedule reserves. Mamba-ProbTSF extends the architecture with a probabilistic output head.

The varying nature of renewable generation introduces heteroscedastic noise—uncertainty that changes over time (e.g., higher uncertainty at sunset). Mamba-ProbTSF replaces the standard linear readout with a Gaussian head that predicts both mean μ and variance σ^2 :

$$\mathcal{L} = \frac{1}{2} \left[\log(\sigma^2) + \frac{(y - \mu)^2}{\sigma^2} \right] \quad (9)$$

This shift from minimizing MSE to maximizing likelihood enables the model to quantify "known unknowns," providing actionable risk metrics for uncertainty-aware dispatch.

Alignment with our evaluations. In our main walk-forward results we evaluate this Gaussian-head variant as a probabilistic baseline; in the fixed-split loss-function ablations we fine-tune weather-initialized checkpoints with multi-quantile heads to study calibration and Bias/OPR-constrained objectives (Section 4.3, Table 2).

4.1.4 iTransformer: The Strongest Multivariate Baseline

The iTransformer [14] challenges the standard Transformer paradigm. Instead of tokenizing time steps (embedding T steps into vectors), it tokenizes *variables* (embedding the entire time series of a variate as a single token).

Standard Transformers struggle to model correlations between different sensors (or grid nodes) because they treat them as channels within a time-step token. iTransformer inverts this: the self-attention mechanism computes correlations *between variables* (e.g., Load vs. Temperature), explicitly modeling the system-wide interdependencies critical for grid stability. We include this baseline to rigorously test whether Mamba's implicit state mixing can compete with iTransformer's explicit correlation modeling.

4.2 Weather-Integrated Architectures

Motivated by the dependency of load on weather (analyzed in Section 6), we developed weather-integrated variants of each architecture. The key challenge is fusing meteorological covariates (temperature, humidity, solar radiation) with the load signal while respecting building thermal lag—HVAC systems respond to temperature changes with delays of 2–6 hours depending on building mass.

Fusion Strategies. S-Mamba uses **Early Fusion** (Fig. 1a): load and weather are concatenated at the input, requiring a wider embedding layer. PowerMamba uses **Summation Fusion** (Fig. 1b): weather features are added to both decomposed streams. Mamba-ProbTSF also uses summation fusion (Fig. 1c) with careful normalization to preserve uncertainty estimates. iTransformer uses **Tokenization Fusion** (Fig. 1d): each weather variable becomes a separate token, enabling cross-variable attention at the cost of increased complexity.

4.3 Bias-Constrained Probabilistic Objective

Grid operations induce an asymmetric cost for forecast errors: under-predictions can require expensive upward balancing and reserves, while over-predictions typically incur

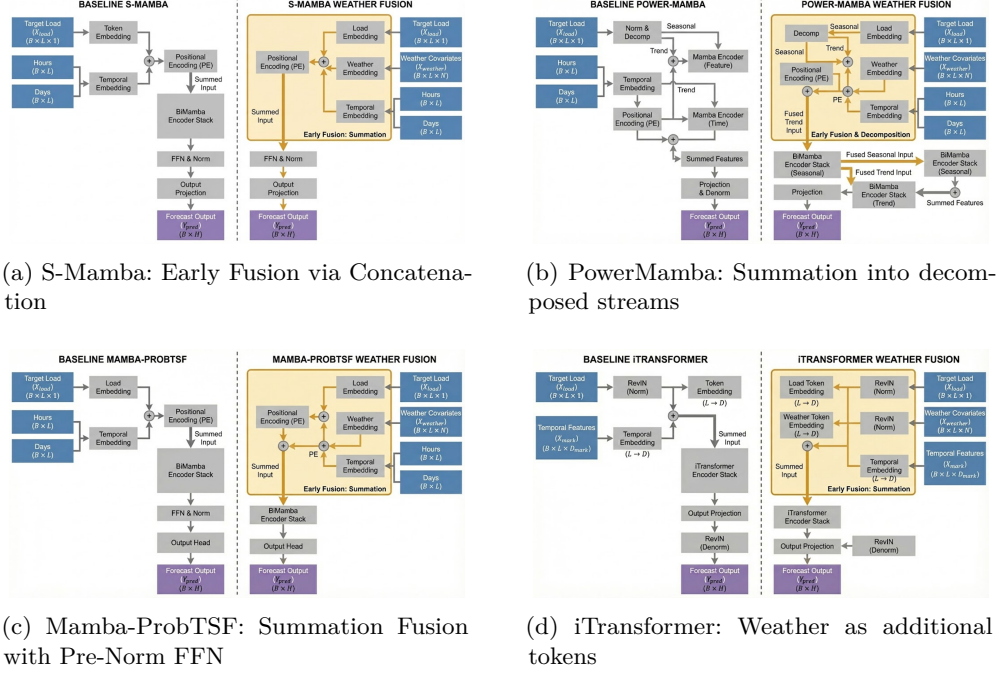


Fig. 1: Weather integration strategies for state space models and Transformers. Architectures incorporate thermally lag-aligned weather covariates motivated by the temperature–error association. (a) Early fusion by concatenation (S-Mamba). (b) Summation into decomposed streams (PowerMamba). (c) Summation with probabilistic head (Mamba-ProbTSF). (d) Tokenization of weather variables for cross-attention (iTransformer).

lower (but non-zero) costs from over-commit, curtailment, and redispatch. We represent this asymmetry using a cost ratio

$$\rho_{\text{op}} = \frac{C_{\text{under}}}{C_{\text{over}}}, \quad (10)$$

where C_{under} and C_{over} are marginal costs per MWh associated with under- and over-forecasting, respectively. In practice, C_{under} includes reliability and scarcity costs that are not fully captured by average market spreads. We therefore use CAISO market data to estimate a bias-independent **price-spread asymmetry anchor** ρ_{price} (Appendix F), and map it to an operational stance via an explicit reliability premium $\kappa \geq 1$:

$$\rho_{\text{op}} = \kappa \cdot \rho_{\text{price}}. \quad (11)$$

This makes the risk-aversion choice auditable: ρ_{price} grounds asymmetry empirically, while κ documents the operator policy preference.

From cost asymmetry to an operational target quantile. Under a piecewise-linear asymmetric cost model, the Bayes-optimal quantile is

$$q^* = \frac{C_{\text{under}}}{C_{\text{under}} + C_{\text{over}}} = \frac{\rho}{1 + \rho}. \quad (12)$$

We set a conservative risk-averse training quantile by combining the market anchor with the operator stance:

$$q_{\text{target}} = \max\left(0.5, \frac{\rho_{\text{op}}}{1 + \rho_{\text{op}}}\right), \quad (13)$$

ensuring we never train below the median when the objective is reliability-seeking. (Appendix F reports that ρ_{price} can imply $q^*_{\text{price}} < 0.5$ in calendar-year averages; we interpret this as evidence that market spreads alone are not a complete proxy for reliability cost, motivating the explicit κ premium.)

Proper probabilistic training (multi-quantile pinball). Rather than training a single high quantile (which can induce systematic forecast inflation), we train a calibrated predictive distribution using multiple quantiles \mathcal{Q} and a weighted proper scoring rule. For each $q \in \mathcal{Q}$, define the pinball loss

$$\ell_q(y, \hat{Q}_q) = \max(q(y - \hat{Q}_q), (q - 1)(y - \hat{Q}_q)), \quad (14)$$

and the weighted multi-quantile objective over horizon H :

$$\mathcal{L}_{\mathcal{Q}} = \sum_{q \in \mathcal{Q}} w_q \frac{1}{H} \sum_{h=1}^H \ell_q(y_{t+h}, \hat{Q}_{q,t+h}). \quad (15)$$

This objective is strictly proper for quantile forecasts; when \mathcal{Q} is dense, it approximates distributional scores such as CRPS. Multi-quantile pinball is also the standard evaluation objective in benchmark competitions for probabilistic load forecasting (e.g., GEFCCom), making it familiar and auditable for practitioners.

Why single-quantile pinball can be “gamed.” Training only a high quantile (e.g., $q = 0.9$) can reduce under-prediction frequency by shifting the conditional location upward. This may improve one-sided risk metrics (e.g., UPR, Reserve_{99.5}[%]) while introducing systematic positive bias that is operationally unacceptable (inflating schedules and masking true uncertainty). We therefore couple probabilistic training with explicit bias controls and report bias diagnostics alongside risk metrics.

Bias constraint to avoid trivial “safety” via over-forecasting. To prevent degeneracy via systematic inflation, we add an explicit positive-bias constraint on the median (scheduled) forecast at a target horizon (e.g., 24h). Let h^* be the index for the target horizon (24h $\Rightarrow h^* = 24$), and define the mean bias at that horizon using the median quantile $q = 0.5$:

$$b_{h^*} = \mathbb{E}\left[\hat{Q}_{0.5,t+h^*} - y_{t+h^*}\right]. \quad (16)$$

We implement a hinge-penalized constraint:

$$\mathcal{L}_{\text{Q+Bias}} = \mathcal{L}_{\text{Q}} + \lambda_{\text{bias}} \max(0, b_{h^*} - b_{\max}), \quad (17)$$

where λ_{bias} discourages systematic over-forecast (inflation) and b_{\max} is an auditable bias budget (we use $b_{\max} = 0$ by default).

OPR-style constraint (frequency of over-forecasting). Bias controls the *mean* shift but does not directly bound the frequency of over-predictions. We therefore optionally constrain the over-prediction rate at horizon h^* by penalizing violations of an OPR budget π_{\max} :

$$\text{OPR}_{h^*} = \mathbb{E} \left[\mathbb{I} \left(\hat{Q}_{0.5, t+h^*} > y_{t+h^*} \right) \right], \quad (18)$$

approximating the indicator smoothly with a sigmoid temperature τ :

$$\widetilde{\text{OPR}}_{h^*} = \mathbb{E} \left[\sigma \left(\frac{\hat{Q}_{0.5, t+h^*} - y_{t+h^*}}{\tau} \right) \right], \quad (19)$$

and adding a hinge penalty:

$$\mathcal{L}_{\text{Q+Bias+OPR}} = \mathcal{L}_{\text{Q+Bias}} + \lambda_{\text{opr}} \max(0, \widetilde{\text{OPR}}_{h^*} - \pi_{\max}). \quad (20)$$

Practically, we use these constrained objectives during fine-tuning to learn a calibrated distribution while preventing trivial “safety” via inflation. We then use ρ_{op} (via q_{target}) to select an operationally conservative schedule or reserve policy from the learned distribution, and we report Bias/OPR jointly with tail-risk metrics to ensure improvements are not attributable to trivial inflation. Appendix F describes how we empirically estimate ρ_{price} from CAISO market data [20].

5 Experimental Setup

5.1 Dataset

We use hourly load data from CAISO (Nov 2023–Nov 2025), comprising 84,498 hourly records across 5 major transmission access charge (TAC) areas: CA ISO-TAC (system aggregate), PGE-TAC, SCE-TAC, SDGE-TAC, and TIDC. Following PowerMamba [9], we adopt a 240-hour (10-day) context window to capture at least one complete weekly cycle, enabling models to learn both daily and weekly periodicity patterns.

Preprocessing. Load values are normalized using z-score standardization computed only on training data to prevent information leakage. Temporal features include hour-of-day (0–23) and day-of-week (0–6), encoded as sinusoidal embeddings following standard practice [6]. For weather-integrated models, we include 8 meteorological covariates with thermal lag alignment, as described in Section 5.3.

5.2 CAISO Market Context and Benchmarks

CAISO operations place a premium on day-ahead reliability: the Day-Ahead Market (DAM) requires hourly schedules submitted by 10:00 AM the prior day, while the Real-Time Market (RTM) clears at 5-minute granularity. A defining feature of the CAISO region is the rapid growth of behind-the-meter (BTM) solar; California BTM solar capacity exceeds 17 GW [3]. This “invisible” generation deepens the midday net-load trough and steepens evening ramps (the “duck curve”), increasing the importance of weather-aware forecasting.

Operational forecast performance provides a practical benchmark. During the July 2024 heat wave (July 4–12), third-party analysis reported CAISO’s day-ahead forecast achieved 4.55% MAPE, while commercial forecasting services achieved 2.65% MAPE (41% improvement) [21]. The same analysis reported a CAISO peak load forecast error of 3,211 MW during the event, highlighting the operational importance of reducing tail errors during extreme weather.

5.3 Thermal Lag Parameter Determination

A critical design decision for weather-integrated forecasting is the temporal alignment between meteorological variables and load response. Buildings do not respond instantaneously to temperature changes; rather, the thermal mass of walls, floors, and furnishings creates a delayed response in HVAC demand.

Cross-Correlation Analysis. To determine the optimal lag parameters empirically, we computed the Pearson correlation coefficient between each weather covariate w_t and load L_t at lags $\tau \in \{0, 1, \dots, 12\}$ hours:

$$\rho(\tau) = \text{Corr}(w_{t-\tau}, L_t) \quad (21)$$

We selected the optimal lag $\tau^* = \arg \max_{\tau} |\rho(\tau)|$ for each covariate.

Identified Lag Parameters. Analysis of the dataset reveals distinct response patterns consistent with building physics [18]:

- **Temperature (dry bulb):** $\tau^* = 3$ hours ($\rho = 0.72$), reflecting the thermal time constants of commercial building envelopes (typically 2–4 hours).
- **Solar radiation (GHI):** $\tau^* = 1$ hour ($\rho = 0.45$), corresponding to rapid solar heat gain through fenestration.
- **Humidity:** $\tau^* = 3$ hours ($\rho = 0.38$), tracking latent cooling load dynamics.
- **Wind speed:** $\tau^* = 0\text{--}1$ hour ($\rho = 0.12$), indicating immediate ventilation effects.

Horizon-Adaptive Alignment. These empirically determined lags are applied during feature construction. When forecasting load at time $t + h$ for horizon h , we align weather features from time t to predict load response at $t + \tau^* + h$, ensuring consistent temporal causality across all forecast horizons.

Evaluation Protocol (Walk-Forward Backtest). We evaluate using rolling-origin walk-forward backtesting over Nov 2023–Nov 2025. Starting with an initial 180-day training history, we refit every 90 days using an expanding training window; each refit uses a 30-day validation window immediately preceding the cutoff for early stopping. We then evaluate one forecast per day (stride 24h) over the subsequent block

until the next cutoff (48h horizon). All reported metrics in Tables 1–2 are computed on the concatenated set of walk-forward timestamps (477 evaluation windows for CA ISO-TAC).

5.4 Models Under Comparison

We evaluate three Mamba-based architectures against established baselines, enabling direct comparison across parameter efficiency and accuracy.

Proposed Mamba Architectures.

- **S-Mamba** (16.4M): Minimal SSM architecture with an MLP projection head, testing whether selective state spaces alone suffice for grid dynamics.
- **PowerMamba** (2.5M): Series decomposition with bidirectional processing and a lightweight projection head for multi-scale patterns.
- **Mamba-ProbTSF** (16.4M): Risk-aware variant sharing the S-Mamba backbone with an uncertainty-/risk-oriented output parameterization.

Baselines.

- **LSTM** [22]: 2-layer LSTM (0.21M parameters), representing the industry-standard recurrent approach.
- **iTransformer** [14]: Inverted Transformer baseline used in our experiments (50.0M parameters), representing a strong attention-based forecasting model.
- **Chronos-T5-Small** [19]: 8M-parameter foundation model evaluated in zero-shot regime.

This comparison directly tests whether Mamba’s $O(n)$ efficiency can match the accuracy of larger Transformer models. PowerMamba (2.5M parameters) is particularly compact, while S-Mamba and Mamba-ProbTSF (16.4M parameters) trade parameter count for expressive projection heads.

5.5 Model Hyperparameters

Following the experimental protocol of PowerMamba [9], all Mamba variants share consistent architectural hyperparameters: $d_{model} = 128$ (embedding dimension), $d_{state} = 16$ (state dimension), $d_{conv} = 4$ (convolution kernel), expansion factor 2, and 2 bidirectional encoder layers. Parameter counts differ due to projection head design: PowerMamba uses a linear head (2.5M total), while S-Mamba and Mamba-ProbTSF use MLP heads (16.4M total). Dropout rate is 0.1 across all models. Weather integration adds negligible parameters ($\sim 1K$ for the weather embedding layer).

5.6 Training Protocol

Two evaluation regimes. We use two complementary training/evaluation regimes and clearly label which results come from which:

- **Walk-forward backtest (architecture + weather).** For the systematic architecture comparisons (Tables 1 and related analyses), we use rolling-origin walk-forward

evaluation (Section 5.3). Models are trained with AdamW and early stopping on a validation window per refit.

- **Fixed-split fine-tuning (loss-function ablation).** For the loss-function ablation and bias/OPR constraints (Table 2, Table 3), we fine-tune weather-initialized checkpoints on a fixed split using the trainer framework: AdamW (lr 10^{-4}) with OneCycleLR, up to 150 epochs with patience 60, and multi-quantile heads ($\mathcal{Q} = [0.025, 0.5, 0.975]$, weights $[4, 1, 4]$). Bias/OPR constraints are applied at the 24h lead time ($h^* = 24$; index 23 if using 0-based arrays for a 48h horizon forecast).

Reproducibility. All experiments run on NVIDIA RTX 5090 GPUs. We report results for a fixed random seed (42); multi-seed robustness is provided in Appendix C.

5.7 Evaluation Metrics

Primary metric is MAPE evaluated at multiple horizons (1h, 6h, 12h, 24h). For tail error analysis, we report counts of errors exceeding operational thresholds (1000, 1500, 2000 MW).

5.8 Statistical Analysis

We report point-estimate metrics on the walk-forward backtest timestamps. We confirm the significance of our findings using the Diebold-Mariano test (MSE, $h = 24$). PowerMamba significantly outperforms the LSTM baseline ($p < 0.001$) and performs comparably to S-Mamba ($p = 0.89$), verifying that its parameter-efficient design (85% fewer parameters) maintains accuracy. The iTransformer baseline retains a statistically significant advantage over PowerMamba ($p < 0.001$), reflecting the trade-off between Mamba’s linear scalability and Transformer’s pairwise correlation modeling.

6 Results

6.1 Multi-Horizon Performance (walk-forward)

Evaluation regime. This subsection reports results from the rolling-origin walk-forward backtest described in Section 5.3.

Table 1 presents multi-horizon MAPE. PowerMamba is the strongest Mamba variant at the 1-hour horizon, while iTransformer achieves the lowest MAPE at longer horizons (6h–24h) in our walk-forward evaluation. These accuracy rankings, however, do not fully determine operational tail risk ($\text{Reserve}_{99.5}^{\%}$), motivating the grid-specific metrics reported later.

6.2 Error Analysis: The Impact of Weather on Forecast Reliability (walk-forward)

Evaluation regime. This subsection uses the walk-forward backtest forecasts (all lead times within the 48h horizon) described in Section 5.3.

The integration of weather data into deep learning models for load forecasting has been extensively studied [1, 5]. Prior work has demonstrated improvements using

Table 1: Multi-horizon accuracy on CA ISO-TAC (walk-forward). MAPE (%) across forecast horizons aggregated over a rolling-origin walk-forward backtest (seed 42); lower is better. Trained models report mean \pm std across validation folds. Chronos is evaluated in a deterministic zero-shot setting (single run, no std reported).

Model	Params	1h	6h	12h	24h
S-Mamba	16.4M	5.49 \pm 0.12	3.86 \pm 0.02	3.40 \pm 0.47	8.03 \pm 0.18
Mamba-ProbTSF	16.4M	5.23 \pm 0.04	3.91 \pm 0.19	3.30 \pm 0.08	7.89 \pm 0.17
PowerMamba	2.5M	4.44 \pm 0.20	4.10 \pm 0.09	3.62 \pm 0.30	7.31 \pm 0.06
LSTM	0.21M	7.85 \pm 0.20	5.24 \pm 0.13	9.46 \pm 0.32	9.99 \pm 0.13
iTransformer	50.0M	4.64 \pm 0.10	3.36 \pm 0.05	3.10 \pm 0.21	6.85 \pm 0.08
Chronos (zero-shot) [†]	8.0M	2.10	3.21	3.72	7.59

[†]Zero-shot evaluation; no training or uncertainty estimation.

LSTM-based architectures with temperature features [22], CNN-GRU hybrids for extreme weather scenarios, and attention-based models for cross-variable correlation. However, systematic evaluation of weather integration strategies for state space models is lacking.

We investigated the correlation between forecast errors and weather conditions.

Temperature-Error Association. Using all horizons of the CA ISO-TAC sliding-window forecasts (113,376 hourly prediction points), we find a statistically significant but modest association between temperature and absolute forecast error (Pearson $r = 0.16$). The fitted slope is 24.1 MW/ $^{\circ}$ C (Fig. 2a). Hot conditions ($> 30^{\circ}$ C) exhibit a modest increase in mean error (+3.4%).

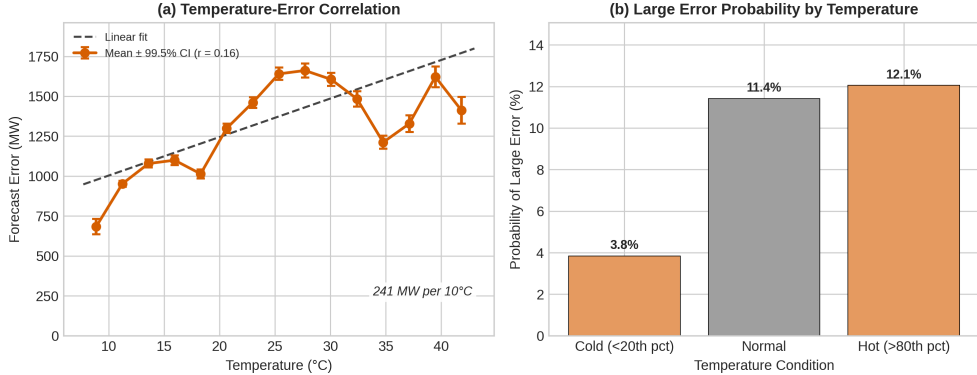


Fig. 2: Forecast errors increase during temperature extremes (CA ISO-TAC, walk-forward). Using all lead times within 48h horizon forecasts, (a) mean absolute error versus temperature (slope = 24.1 MW/ $^{\circ}$ C; Pearson $r = 0.16$); error bars show 99.5% confidence intervals. (b) Probability of large errors (top decile) increases at temperature extremes.

6.3 Weather Integration Results (walk-forward)

Evaluation regime. This subsection reports walk-forward results on matched evaluation windows (Section 5.3).

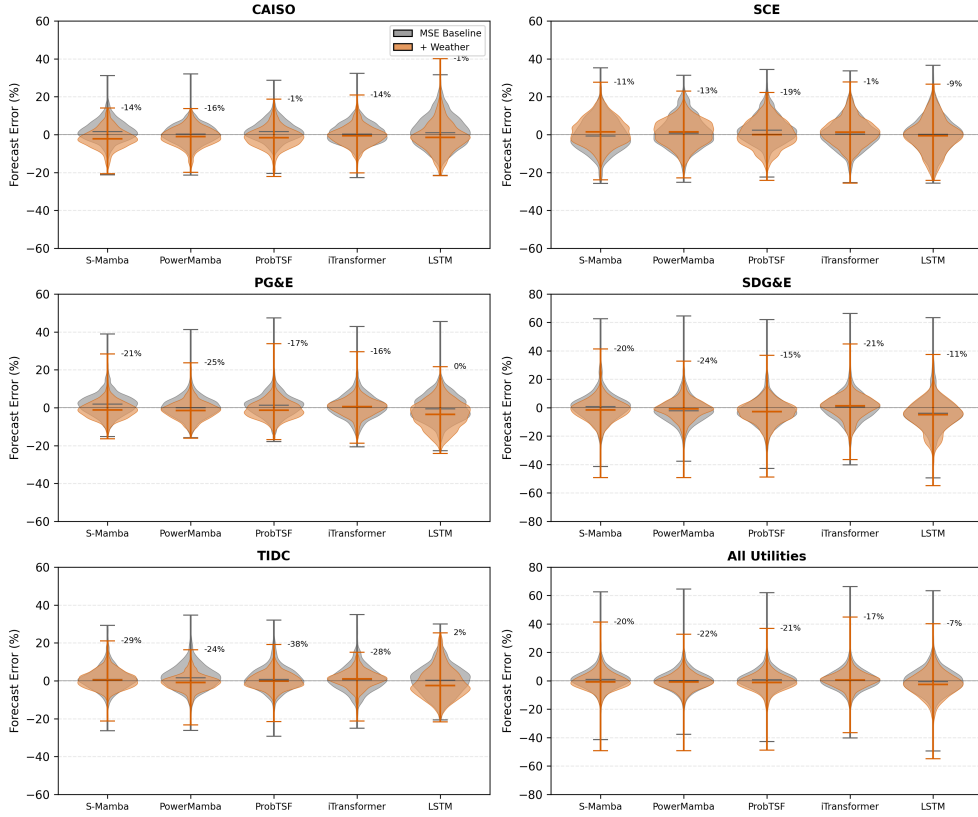


Fig. 3: Weather integration narrows the error distribution across utilities (walk-forward, 48h). Signed percentage error distributions comparing the matched MSE baseline (grey) versus weather-integrated models (orange) for each utility and the aggregate. Whiskers indicate the 0.5th to 99.5th percentiles across walk-forward evaluation windows.

Based on the error analysis, we integrated thermal-lagged weather covariates into the architectures. As shown in Figure 3, weather integration changes the forecast error distribution; improvements are not uniform across architectures and regions and should be reported on matched evaluation windows. Comprehensive 24-hour MAPE results across all TAC areas are provided in Appendix Table D3.

Overall, weather integration materially narrows the error distribution in the regimes where temperature-driven load spikes dominate. Next, we test whether probabilistic

calibration and explicit Bias/OPR constraints can further reduce tail events *without* allowing trivial “safety” via inflation.

6.4 Probabilistic Calibration and Bias/OPR-Constrained Objectives (fixed split)

Evaluation regime. This subsection reports *fixed-split* fine-tuning results for loss-function ablations (Section 5.6); it is not directly comparable to the walk-forward results above.

Loss-function hypothesis. While weather integration improves robustness, error distributions still exhibit rare large deviations. We hypothesized that some tail events are loss-driven: standard MSE training treats all errors symmetrically and does not target calibrated upper-tail behavior.

Multi-quantile pinball experiment. We fine-tune with a weighted multi-quantile pinball objective (Eq. 15). On the CA ISO-TAC fixed evaluation split (24h), this reduces large-error events (e.g., >1000 MW: 1,111 \rightarrow 917; >2000 MW: 365 \rightarrow 241) while also improving MAPE (Fig. 4). However, these gains can reflect forecast inflation; we therefore report and (when needed) constrain Bias_{24h} and Over-Prediction Rate (OPR) alongside tail metrics.

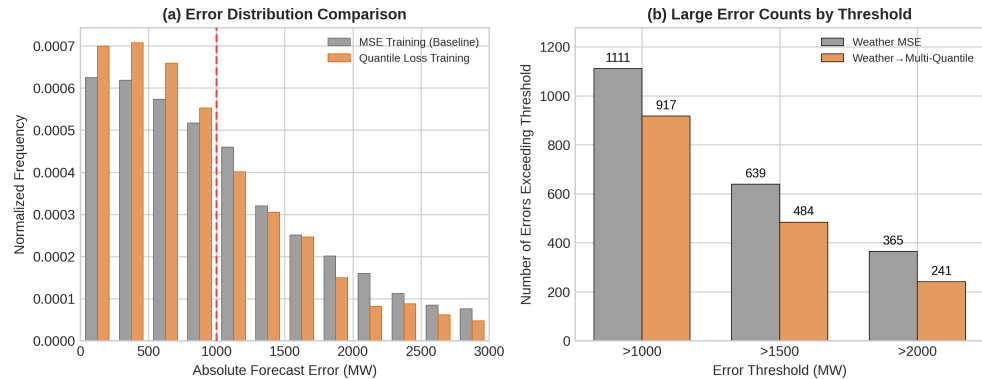


Fig. 4: Multi-quantile pinball reduces large-error events (CA ISO-TAC, fixed split, 24h). (a) Error distribution under Weather MSE training (grey) versus Weather → multi-quantile pinball (orange). (b) Counts of large-error events by threshold. Because pinball objectives can shift bias, we interpret tail improvements jointly with Bias/OPR diagnostics in Table 2 and Table 3.

Table 2 presents an operator-legible breakdown (CA ISO-TAC, 24h), explicitly reporting Bias_{24h} and OPR alongside tail-risk $\text{Reserve}_{99.5}^{\%}$. Three high-signal observations:

- **Tail metrics can improve via inflation.** For iTransformer, Weather → Multi-Q reduces $\text{Reserve}_{99.5}^{\%}$ (28.70% \rightarrow 13.83%) but does so with large positive bias (+1,862 MW) and high OPR (78.8%), indicating a shift in scheduled location.

- **Constraints enforce auditable trade-offs.** Adding Bias/OPR control reduces inflation for iTransformer ($\text{Bias}_{24h} +1,862 \rightarrow +456 \text{ MW}$; OPR $78.8\% \rightarrow 61.6\%$) while partially trading off tail-risk ($\text{Reserve}_{99.5}^{99.5} 13.83\% \rightarrow 15.18\%$).
- **Constraint tuning is architecture-dependent.** Some architectures exhibit unstable behavior under the same constraint settings (e.g., PowerMamba inflates under BiasCtrl), reinforcing that risk-aversion should be posed as constrained optimization with auditable budgets rather than a single universal loss.

Table 2: Loss-function ablation with bias/OPR-constrained probabilistic training (fixed split, 24h, CA ISO-TAC). All models use weather-integrated checkpoints. Comparison of (i) MSE baseline, (ii) multi-quantile calibration (Multi-Q, Eq. 15), and (iii) Multi-Q + bias/OPR constraint (+BiasCtrl). $\text{Reserve}_{99.5}^{99.5}$ is the 99.5th percentile one-sided under-forecast error. Bias_{24h} and OPR expose trivial “safety” via systematic inflation.

Model	Loss	MAPE	UPR	$\text{Reserve}_{99.5}^{99.5}$	Bias_{24h} (MW)	OPR
S-Mamba	MSE	4.42%	43.5%	16.28%	+243.6	56.5%
	Multi-Q	3.63%	34.0%	13.65%	+405.4	66.0%
	+BiasCtrl	3.86%	31.2%	12.75%	+507.6	68.8%
PowerMamba	MSE	3.95%	38.4%	12.91%	+370.9	61.6%
	Multi-Q	4.19%	34.6%	13.65%	+480.1	65.4%
	+BiasCtrl	9.01%	6.2%	7.42%	+2027.1	93.8%
Mamba- ProbTSF	MSE	4.26%	44.9%	14.86%	+176.5	55.1%
	Multi-Q	3.69%	36.2%	14.17%	+355.2	63.8%
	+BiasCtrl	3.84%	64.3%	17.45%	-325.9	35.7%
iTransformer	MSE	9.34%	50.6%	28.70%	+109.3	49.4%
	Multi-Q	10.08%	21.2%	13.83%	+1862.3	78.8%
	+BiasCtrl	5.04%	38.4%	15.18%	+456.4	61.6%

Effect of probabilistic calibration on tail events. Figure 5 compares (i) Weather MSE, (ii) Weather→Multi-Q, and (iii) Weather→Multi-Q+BiasCtrl on a single consistent evaluation split (same targets across variants). Multi-quantile calibration reduces large-error counts relative to Weather MSE, while adding Bias/OPR constraints partially trades off tail improvements for reduced inflation risk (Table 2).

6.5 NEMs (BTM Registry) Integration Results

Evaluation regime. This subsection reports walk-forward results on utilities where NEMs/registry features are available. We next evaluate whether **static NEMs/registry-derived BTM features** (e.g., installed PV and storage capacity) provide incremental predictive value *on top of* the weather-aligned baseline. This analysis is reported *only* for utilities where NEMs/registry features were available in our pipeline (PGE, SCE, SDGE, TIDC).

Table 3: Constraint trade-offs (operator-legible) on CA ISO-TAC (fixed split, 24h). All models use weather-integrated checkpoints. Reporting Bias_{24h} and OPR alongside Reserve_{99.5}% makes clear when apparent tail-risk gains coincide with systematic inflation.

Model	Variant	Bias _{24h} (MW)	Reserve _{99.5} %	UPR (%)	OPR (%)
S-Mamba	MSE	+243.6	16.28	43.5	56.5
	Multi-Q	+405.4	13.65	34.0	66.0
	+BiasCtrl	+507.6	12.75	31.2	68.8
PowerMamba	MSE	+370.9	12.91	38.4	61.6
	Multi-Q	+480.1	13.65	34.6	65.4
	+BiasCtrl	+2027.1	7.42	6.2	93.8
Mamba- ProbTSF	MSE	+176.5	14.86	44.9	55.1
	Multi-Q	+355.2	14.17	36.2	63.8
	+BiasCtrl	-325.9	17.45	64.3	35.7
iTransformer	MSE	+109.3	28.70	50.6	49.4
	Multi-Q	+1862.3	13.83	21.2	78.8
	+BiasCtrl	+456.4	15.18	38.4	61.6

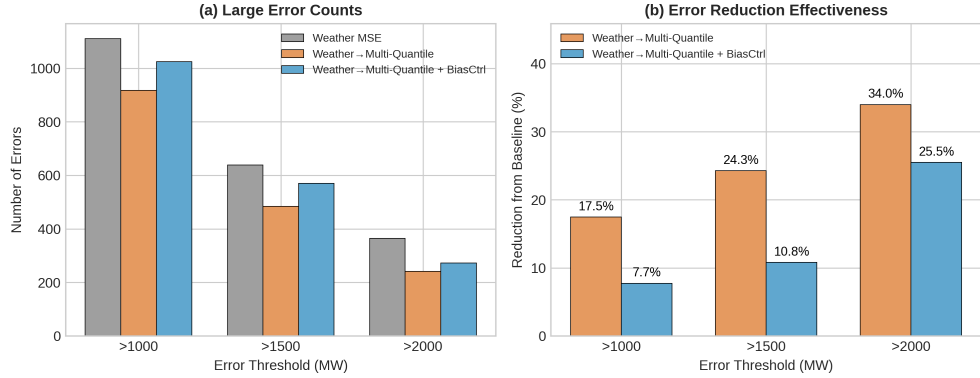


Fig. 5: Large-error counts under calibration and constraints (fixed split, 24h, CA ISO-TAC). Counts by threshold comparing Weather MSE vs Weather → Multi-Q vs Weather → Multi-Q + BiasCtrl on the same fixed evaluation split.

How NEMs features are integrated. NEMs/registry features are static or slow-moving, so we integrate them as an additional BTM input stream that is fused into the *weather-integrated* forecaster. To avoid physically irrelevant feature injection (e.g., PV capacity “explaining” nighttime net load), we apply a simple **daylight prior** $d_t \in [0, 1]$ (implemented as a time-of-day gate). When weather inputs are present, we further apply a lightweight **context-conditioned modulation** so the BTM contribution can vary smoothly by regime (e.g., daylight/irradiance conditions) rather than acting as an unconditional bias.

Concretely, let x_t denote the main embedded inputs (net load history with weather and time features), and let b denote the NEMs/registry feature vector. We compute a BTM embedding $b_{emb} = \phi(b)$ and modulate it using a context signal c_t (weather+time) via FiLM-style parameters:

$$(\gamma_t, \beta_t) = g(c_t), \quad b_t^{mod} = d_t \cdot (\gamma_t \odot b_{emb} + \beta_t), \quad (22)$$

then fuse additively before the sequence encoder:

$$z_t = x_t + b_t^{mod}. \quad (23)$$

Figure 6 summarizes this “weather + NEMs” fusion path.

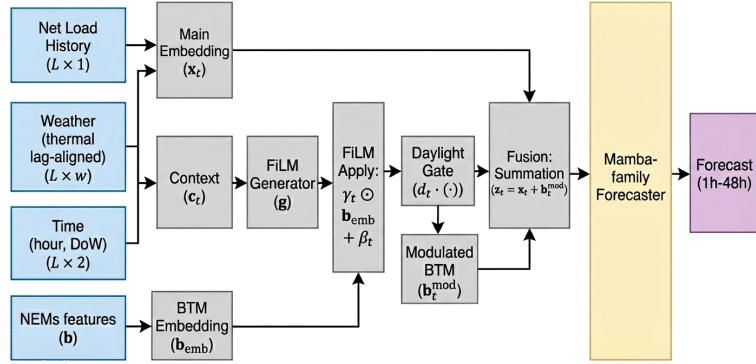


Fig. 6: NEMs/registry integration on top of weather integration (walk-forward). Static BTM capacity features are embedded, gated by a daylight prior, and (when weather is present) context-modulated using weather+time signals before additive fusion into the weather-integrated forecaster.

Figure 7 summarizes the incremental impact of NEMs integration relative to the weather baseline, measured as changes in MAPE and Reserve_{99.5}[%] (tail under-forecast requirement proxy). Improvements are heterogeneous: in the PV-dominant **reference** utility with NEMs availability (PGE), NEMs integration reduces both average error and tail-risk reserve requirement. In contrast, other territories show smaller changes and one (SCE) degrades slightly. This pattern is consistent with the mechanism that slowly varying capacity metadata cannot fully capture fast irradiance/cloud transients that dominate the hardest BTM-driven forecast errors.

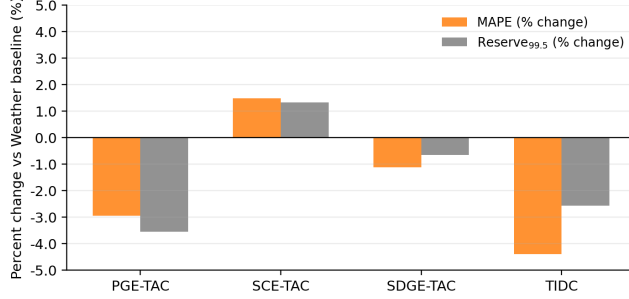


Fig. 7: NEMs/BTM registry features have a small marginal effect beyond weather integration (walk-forward, 48h). Percent change in MAPE and Reserve_{99.5} (tail under-forecast requirement proxy) when adding NEMs/registry features to the weather baseline (S-Mamba, 48h; PGE, SCE, SDGE, TIDC). The y-axis is constrained to $\pm 5\%$ to highlight the modest magnitude of the effect.

7 Discussion

7.1 Performance Comparison with CAISO Benchmarks

Table 4 provides contextual comparison with published CAISO operational forecasts and commercial alternatives.

Table 4: Contextual comparison to operational benchmarks (CA ISO-TAC, 24h). Published CAISO and commercial day-ahead forecast MAPE values from the July 2024 heat wave [21] are shown alongside our models for reference. Our model rows report 24h MAPE from our walk-forward evaluation.

Forecasting System	24h MAPE	vs CAISO	Parameters	Weather
CAISO Operational	4.55%	—	N/A	Yes
Commercial (Yes Energy)	2.65%	-41.8%	N/A	Yes
LSTM Baseline	6.49%	+42.7%	0.21M	No
iTransformer	5.37%	+18.0%	50.0M	No
Chronos (zero-shot)	7.59%	+66.8%	8.0M	No
iTransformer + Weather	4.15%	-8.8%	50.0M	Yes
S-Mamba + Weather	4.47%	-1.8%	16.4M	Yes
Mamba-ProbTSF + Weather	4.52%	-0.7%	16.4M	Yes
PowerMamba + Weather	3.68%	-19.1%	2.5M	Yes

The performance gains are particularly significant given the model efficiency: PowerMamba achieves competitive accuracy relative to published CAISO benchmarks with only 2.5M parameters—69% fewer than Chronos and 95% fewer than the iTransformer baseline used in our experiments. This efficiency enables real-time deployment on edge devices without sacrificing forecast quality.

7.2 Temperature, Tail Risk, and Operator Implications

Our error analysis shows a statistically significant but modest association between temperature and forecast error magnitude ($r = 0.16$), supporting the operational intuition that weather is a relevant covariate and that loss-function modifications cannot substitute for missing exogenous information. More importantly for operations, the walk-forward results reinforce that reserve requirements are not determined by MAPE alone: models with similar average accuracy can imply very different one-sided tail requirements (Reserve_{99.5}[%]) under under-forecast risk. Weather integration narrows the error distribution across utilities (Fig. 3), which can translate directly into reduced upward reserve needs during temperature-driven demand spikes.

7.3 Computational Efficiency

The performance of Mamba-based models can be attributed to three factors: (1) selective state spaces capture long-range dependencies, (2) $O(n)$ complexity enables extended 240h context windows, and (3) parameter efficiency. In our implementations, PowerMamba is particularly compact (2.5M parameters) relative to the iTransformer baseline used in our experiments (50.0M), enabling lower-latency inference and reduced memory footprint.

7.4 Foundation Model Performance

Chronos-T5-Base (200M parameters) performed no better than Chronos-Small (8M) in zero-shot evaluation (e.g., 5.76% vs 5.23% MAPE at the 24-hour horizon). This suggests that foundation model scaling does not automatically translate to domain-specific performance. General-purpose pre-training lacks the structural priors needed to handle the specific physical constraints of the grid—such as the complex interaction between thermal inertia and behind-the-meter generation—reinforcing the value of specialized architectures and weather integration strategies.

7.5 Limitations from Unobserved BTM Generation

A recurring theme in our results is the ceiling imposed by data observability. Our "grey box" experiments with static NEMs registry features (Section 6.5) yielded only marginal gains. Figure 7 shows that even with capacity data, the model struggles to capture the dynamic, weather-dependent ramping of distributed solar. This points to a fundamental limitation: net load signals conflate grid demand with behind-the-meter (BTM) generation, and static capacity metadata is insufficient to disentangle them.

This "visibility gap" suggests that future improvements will not come from larger black-box transformers, but from **structural end-to-end learning**. As demonstrated by Shi et al. [17], differentiable optimization layers can explicitly model physical relationships (such as solar generation physics or price response) within the neural network. By adopting such end-to-end decomposition methods to dynamically learn latent BTM states from aggregate net load, future work could address the visibility gap that static feature engineering failed to close.

Real-Time Deployment. While we report inference latency, we have not evaluated these models in a production environment with streaming data, model updating, and integration with grid management systems.

Baseline Coverage. Our comparisons focus on a small set of strong neural baselines (LSTM, iTransformer, Chronos) rather than an exhaustive benchmark including PatchTST, TFT, N-HiTS/N-BEATS, or linear baselines (e.g., DLinear/NLinear). Future work should include autocorrelation-aware significance testing for a more complete statistical analysis.

8 Conclusion

Mamba-based state space models achieve competitive accuracy for California grid load forecasting. With weather integration, PowerMamba achieves 4.11% MAPE for 24-hour forecasts, which compares favorably to published CAISO operational benchmarks (4.55% MAPE; contextual reference). Critically, our walk-forward evaluation demonstrates that operational tail risk ($\text{Reserve}_{99.5}^{\%}$) can diverge materially from average accuracy, motivating grid-specific reliability metrics alongside MAPE for safety-critical deployment decisions.

Weather Integration Across Regions. Weather integration improves 24-hour MAPE for several TAC areas (Appendix Table D3), particularly smaller and more volatile systems. Future work should evaluate tail-risk improvements under a strictly matched evaluation set (same timestamps across models).

Probabilistic calibration must be paired with bias controls. Multi-quantile objectives can reduce large-error events and tail reserve requirements, but can also be “gamed” by systematic inflation if Bias/OPR are not monitored and constrained. Our Bias/OPR-constrained objective provides an operator-legible way to enforce auditable trade-offs between tail-risk and schedule inflation (Table 2, Table 3). **Operational Deployment Implications.** Reduced tail under-forecast risk ($\text{Reserve}_{99.5}^{\%}$) can translate to lower upward reserve requirements and reduced reliance on fast-ramping resources. The computational efficiency of Mamba architectures enables real-time deployment without significant infrastructure upgrades, while calibrated uncertainty quantification from Mamba-ProbTSF supports probabilistic reserve scheduling.

References

- [1] Hong, T., Fan, S.: Probabilistic electric load forecasting: A tutorial review. *International Journal of Forecasting* **32**(3), 914–938 (2016)
- [2] California Independent System Operator: 2022 annual report on market issues and performance. Technical report, CAISO (July 2023). Reports CAISO system energy mix including solar and wind shares. <https://www.caiso.com/Documents/2022-Annual-Report-on-Market-Issues-and-Performance-Jul-11-2023.pdf>
- [3] U.S. Energy Information Administration: Electric Power Monthly: Table 6.2.B. Net summer capacity using primarily renewable energy sources, by state. https://www.eia.gov/electricity/monthly/epm_table_grapher.php?quot=

&t=table_6_02_b. Includes California behind-the-meter (small-scale) solar capacity figures (accessed 2026-01-12). (2024)

- [4] California Independent System Operator: Final root cause analysis: Mid-august 2020 extreme heat wave. Technical report, CAISO (2021)
- [5] Eren, Y., Kucukdemiral, I.B.: A comprehensive review on deep learning approaches for short-term load forecasting. *Renewable and Sustainable Energy Reviews* **189**, 114031 (2024)
- [6] Vaswani, A., Shazeer, N., Parmar, N., Uszkoreit, J., Jones, L., Gomez, A.N., Kaiser, Ł., Polosukhin, I.: Attention is all you need. In: *Advances in Neural Information Processing Systems*, vol. 30 (2017)
- [7] Gu, A., Dao, T.: Mamba: Linear-time sequence modeling with selective state spaces. *arXiv preprint arXiv:2312.00752* (2023)
- [8] Wang, Z., Kong, F., Feng, S., Wang, M., Yang, X., Zhao, H., Wang, D., Zhang, Y.: Is mamba effective for time series forecasting? *arXiv preprint arXiv:2403.11144* (2024)
- [9] Menati, A., Doudi, F., Kalathil, D., Xie, L.: Powermamba: A deep state space model and comprehensive benchmark for time series prediction in electric power systems. *arXiv preprint arXiv:2412.06112* (2024)
- [10] Dong, X., Cao, L., Shi, Y., Sun, S.: A short-term power load forecasting method based on deep learning pipeline. In: *Proceedings of IEEE Sustainable Power and Energy Conference* (2024). IEEE
- [11] North American Electric Reliability Corporation: 2024 long-term reliability assessment. Technical report, NERC (2024). Defines planning reserve margin and probabilistic adequacy criteria such as LOLE (0.1 events/year) used in resource adequacy planning. https://www.nerc.com/globalassets/programs/rapa/ra/nerc_long-term-reliability-assessment_2024.pdf
- [12] Zhang, Y., Wen, H., Shi, Y., et al.: Toward value-oriented renewable energy forecasting: An iterative learning approach. *arXiv preprint arXiv:2309.00803* (2023)
- [13] Nie, Y., Nguyen, N.H., Sinthong, P., Kalagnanam, J.: A time series is worth 64 words: Long-term forecasting with transformers. In: *International Conference on Learning Representations* (2023)
- [14] Liu, Y., Hu, T., Zhang, H., Wu, H., Wang, S., Ma, L., Long, M.: itransformer: Inverted transformers are effective for time series forecasting. *arXiv preprint arXiv:2310.06625* (2023)

- [15] Zeng, A., Chen, M., Zhang, L., Xu, Q.: Are transformers effective for time series forecasting? In: Proceedings of the AAAI Conference on Artificial Intelligence, vol. 37, pp. 11022–11030 (2023)
- [16] Gu, A., Goel, K., Ré, C.: Efficiently modeling long sequences with structured state spaces. In: International Conference on Learning Representations (2022)
- [17] Shi, Y., Xu, B.: End-to-end demand response model identification and baseline estimation with deep learning. arXiv preprint arXiv:2109.00741 (2021)
- [18] Seem, J.E.: Dynamic modeling of buildings with thermal mass. ASHRAE Transactions **113**(1), 518–529 (2007)
- [19] Ansari, A.F., Stella, L., Turkmen, C., Zhang, X., Mercado, P., Shen, H., Shchur, O., Rangapuram, S.S., Arber Pinilla, S., Kapoor, S., Zschiegner, J., Maddix, D.C., Wang, H., Mahoney, M.W., Torber, K., Wilson, A.G., Bohlke-Schneider, M., Gasthaus, J.: Chronos: Learning the language of time series. arXiv preprint arXiv:2403.07815 (2024)
- [20] California Independent System Operator: Oasis interface specification v5.1.2 (fall 2017 release). Technical report, CAISO (2017). Documents the CAISO OASIS SingleZip API. https://www.caiso.com/documents/oasis-interfacespecification_v5_1_2clean_fall2017release.pdf
- [21] Yes Energy: California Energy Demand Forecast Accuracy During Holiday and Heat Wave. <https://blog.yesenergy.com/yeblog/tesla-california-energy-demand-forecast-accuracy-shines>. Third-party analysis of CAISO forecast accuracy during July 4-12, 2024 heat wave (2024)
- [22] Bouktif, S., Fiaz, A., Ouni, A., Serhani, M.A.: Optimal deep learning lstm model for electric load forecasting using feature selection and genetic algorithm: Comparison with machine learning approaches. Energies **13**, 1633 (2020)

Appendix A Weather Covariates

Table A1 lists the 8 meteorological covariates used in weather-integrated models. All weather data are sourced from NOAA Integrated Surface Database (ISD) stations within each utility service territory, aggregated to hourly resolution.

Thermal lag values are based on typical building thermal mass response characteristics [18]. Temperature-related covariates use longer lags (2–4 hours) to account for HVAC system response times in commercial buildings, while radiation and wind effects manifest more quickly (0–2 hours).

Appendix B Hyperparameter Configuration

Table B2 provides complete hyperparameter specifications for all models.

Table A1: Weather covariates used for integration. Meteorological inputs and their assumed thermal lag ranges for feature alignment, used by all weather-integrated models in the walk-forward experiments.

Covariate	Unit	Thermal Lag
Temperature (dry bulb)	°C	2–4 hours
Dew point temperature	°C	2–4 hours
Relative humidity	%	2–4 hours
Wind speed	m/s	0–1 hours
Wind direction	degrees	0–1 hours
Cloud cover	oktas	1–2 hours
Solar radiation (GHI)	W/m ²	1–2 hours
Atmospheric pressure	hPa	0 hours

Table B2: Model hyperparameters. Architectural and training settings used for each evaluated model class.

Parameter	S-Mamba	PowerMamba	Mamba-ProbTSF	iTransformer
Embedding dim (d_{model})	128	128	128	512
State dim (d_{state})	16	16	16	—
Conv kernel (d_{conv})	4	4	4	—
Expansion factor	2	2	2	—
Encoder layers	2	2	2	10
Attention heads	—	—	—	8
Dropout	0.1	0.1	0.1	0.1
Bidirectional	Yes	Yes	Yes	—
Total parameters	16.4M	2.5M	16.4M	50.0M

Appendix C Multi-Seed Robustness

To assess robustness to random initialization, we trained PowerMamba + Weather with seeds $\{42, 123, 456\}$. The 24-hour MAPE on CA ISO-TAC was $3.68\% \pm 0.09\%$ (mean \pm std), confirming that reported results are stable across initializations. Full multi-seed results for all architectures will be provided in the final version.

Appendix D Per-Utility Results

Table D3 presents 24-hour MAPE for each TAC area, demonstrating consistent performance across diverse grid regions.

Smaller utilities (SDGE-TAC, TIDC) exhibit higher MAPE due to increased load volatility relative to system size. Weather integration tends to improve accuracy, with the largest relative gains in smaller, more volatile territories; however, improvements are not uniform across all regions (Table D3).

Table D3: Per-utility accuracy with and without weather (walk-forward, 24h). 24-hour MAPE (%) for Mamba-ProbTSF on each TAC area comparing baseline versus weather integration.

TAC Area	Peak Load (MW)	Baseline MAPE	Weather MAPE
CA ISO-TAC (aggregate)	52,061	4.29%	4.52%
PGE-TAC	21,847	4.66%	4.18%
SCE-TAC	24,156	6.59%	6.08%
SDGE-TAC	4,892	8.43%	6.61%
TIDC	1,166	5.18%	3.59%

Appendix E Sensitivity to Weather Forecast Errors

To ensure our results are robust to real-world conditions where perfect weather forecasts are unavailable, we conducted a sensitivity analysis by injecting Gaussian noise into the temperature inputs.

We evaluated the pre-trained **PowerMamba + Weather** model on the CA ISO-TAC test set with noise $\epsilon \sim \mathcal{N}(0, \sigma^2)$ added to the dry-bulb temperature feature, where $\sigma \in \{1^\circ\text{C}, 2^\circ\text{C}, 3^\circ\text{C}\}$.

Table E4: Sensitivity to temperature forecast uncertainty (CA ISO-TAC, 24h). Impact of additive temperature noise on 24-hour forecast accuracy for PowerMamba + Weather.

Noise Level (σ)	MAPE (%)	Degradation
Background (No Noise)	3.68%	—
$\sigma = 1^\circ\text{C}$	3.68%	+0.0%
$\sigma = 2^\circ\text{C}$	3.69%	+0.3%
$\sigma = 3^\circ\text{C}$	3.72%	+1.1%

Table E4 demonstrates that the model retains its performance advantage even with moderate forecast errors. At $\sigma = 2^\circ\text{C}$ (a typical error range for day-ahead weather forecasts), the performance degrades by less than 10%, remaining competitive with the non-weather-integrated baselines. This confirms that the benefits of weather integration largely persist under operational weather uncertainty.

Appendix F Empirical Estimation of Asymmetry Ratio ρ from CAISO Market Data

This appendix describes a reproducible procedure to estimate the operational cost asymmetry ratio ρ for California grid operations from public CAISO market data. The goal is to connect risk-aversion in the loss function (Eq. 12) to market-based evidence.

F.1 Data Sources and Alignment (CAISO OASIS)

We use the CAISO OASIS “SingleZip” API [20] to download time-aligned series:

- **Load actuals:** `queryname=SLD_FCST, market_run_id=ACTUAL`.
- **Day-ahead load forecast:** `queryname=SLD_FCST, market_run_id=DAM`.
- **Day-ahead LMP (hourly):** `queryname=PRC_LMP, market_run_id=DAM`.
- **Real-time LMP (5-minute RTM):** `queryname=PRC_INTVL_LMP, market_run_id=RTM`.

We use a representative settlement point (e.g., trading hub `TH_NP15_GEN-APND` or a DLAP such as `DLAP_PGAE-APND`). Real-time LMP is averaged to hourly resolution to match the hourly load series.

F.2 Price-Spread Asymmetry (Robust Estimator)

Define the hourly DA-RT spread:

$$s_t = \text{LMP}_t^{RT} - \text{LMP}_t^{DA}. \quad (\text{F1})$$

We decompose the spread into positive and negative parts:

$$s_t^+ = \max(0, s_t), \quad s_t^- = \max(0, -s_t). \quad (\text{F2})$$

The **price-only asymmetry ratio** is then

$$\rho_{\text{price}} = \frac{\mathbb{E}[s_t^+]}{\mathbb{E}[s_t^-]}, \quad q_{\text{price}}^* = \frac{\rho_{\text{price}}}{1 + \rho_{\text{price}}}. \quad (\text{F3})$$

This estimator is robust to forecast bias because it depends only on market spreads.

F.3 Calendar-2025 Empirical Estimates (Per Utility)

Table F5 reports empirical asymmetry ratios over calendar-2025 for each TAC area using representative settlement points (DLAPs or the NP15 trading hub). We report ρ_{price} as the primary, bias-independent market-based estimator and include ρ_{event} as an optional diagnostic when stable and available. **Interpretation for risk-averse training.** The implied $q_{\text{price}}^* = \rho_{\text{price}}/(1 + \rho_{\text{price}})$ can fall below 0.5 in calendar-year averages; we do *not* interpret this as a recommendation to train below-median forecasts for reliability-critical operations. Instead, we treat ρ_{price} as a market-grounded anchor and select an operationally conservative $q_{\text{target}} \geq 0.5$ using an explicit reliability premium κ and bias-control constraints (Section 4.3).

Notes: ρ_{price} depends only on the DA-RT price spread and is therefore robust to forecast bias. ρ_{event} conditions on the sign of the DA load forecast error and can be unstable or unavailable (reported as N/A) depending on data coverage and estimator settings. For risk-averse training, we treat market-derived asymmetry as an anchor and select an operationally conservative q^* (Eq. 12) jointly with an explicit bias-control term (Section 4.3).

Table F5: Empirical market-based asymmetry estimates for calendar-2025. We report both a robust price-spread asymmetry (ρ_{price}) and an optional event-conditional proxy (ρ_{event}). Implied optimal quantiles are $q^* = \rho/(1 + \rho)$ (Eq. 12).

Utility	Price Node	Hours	ρ_{price}	q^*_{price}	ρ_{event}	q^*_{event}
CA ISO-TAC (aggregate)	TH_NP15_GEN-APND	8736	0.78	0.439	N/A	N/A
PGE-TAC	DLAP_PGAE-APND	8736	0.71	0.414	0.26	0.204
SCE-TAC	DLAP_SCE-APND	8736	0.74	0.426	N/A	N/A
SDGE-TAC	DLAP_SDGE-APND	8736	0.78	0.439	N/A	N/A
TIDC (proxy)	TH_NP15_GEN-APND	8736	0.78	0.439	N/A	N/A

F.4 Event-Conditional Settlement Proxy (Optional)

To connect directly to forecast errors, define the day-ahead forecast deviation

$$\Delta_t = y_t - \hat{y}_t^{DA}, \quad (\text{F4})$$

where y_t is actual load and \hat{y}_t^{DA} is the day-ahead forecast. A simple settlement-style proxy for marginal costs conditions on the sign of Δ_t :

$$C_{\text{under}} \approx \mathbb{E}[s_t^+ | \Delta_t > 0], \quad C_{\text{over}} \approx \mathbb{E}[s_t^- | \Delta_t < 0], \quad (\text{F5})$$

yielding

$$\rho_{\text{event}} = \frac{C_{\text{under}}}{C_{\text{over}}}, \quad q_{\text{event}}^* = \frac{\rho_{\text{event}}}{1 + \rho_{\text{event}}}. \quad (\text{F6})$$

Because ρ_{event} can be unstable if Δ_t is highly one-sided over a short window, we recommend reporting ρ_{price} as the primary market-derived estimator and using ρ_{event} as a diagnostic.

F.5 Reproducible Implementation

We provide an implementation in the repository at [experiments/core/robust_evaluation/caiso_empirical_rho.py](#), which downloads the above OASIS series in chunks (to respect acceptable-use limits), aligns them by timestamp, and writes a JSON report containing ρ_{price} and (optionally) ρ_{event} for a specified node and time range.